Journal of Applied Polymer Science

Tunable molecular weights of poly(triphenylamine-2,2′-bithiophene) and their effects on photovoltaic performance as sensitizers for dye-sensitized solar cells

Haizhen Wang, Wenhui Ding, Gang Wang, Chunyue Pan, Meihong Duan, Guipeng Yu
College of Chemistry and Chemical Engineering, Central South University, Changsha 410083, China
Haizhen Wang and Wenhui Ding contributed equally to this work.
Correspondence to: C. Pan (E-mail: panchunyue@csu.edu.cn) and G. Yu (E-mail: gilbertyu@csu.edu.cn)

ABSTRACT: Despite the huge progress achieved over the past decade, the relationship between the molecular weights of dyes and the performance of dye-sensitized solar cells (DSSCs) remains unclear. In this article, we report on the fine control of the number-average molecular weight (M_n) of poly(triphenylamine-2,2′-bithiophene) (PPAT) dyes with cyanoacrylic acid moieties as acceptors. We found a correlation between the M_n and photovoltaic performance of these polymers when they were used for DSSC applications. In this study, three samples (PPAT-01, PPAT-02, and PPAT-03) with different M_n values (M_ns = 1700, 2800, and 3500 g/mol) were prepared through the control of the polymerization time and characterized by analytical gel permeation chromatography and NMR. Under the same experimental conditions, the overall cell efficiency of the oligomer dyes showed a nonmonotonic tendency with increasing molecular weight. The power-conversion efficiencies were 2.81% for PPAT-01, 4.72% for PPAT-02, and 1.88% for PPAT-03. UV absorption measurements proved that PPAT-03 formed aggregation, whereas PPAT-01 and PPAT-02 were in the monolayer state adsorbed on TiO_2. The larger aggregation decreased charge transfer; thus, poor photoelectric conversion performance was observed. Furthermore, a higher molecular weight reduced the amount of PPAT-03 adsorbed on TiO_2, and this had a crucial effect on the performance of the cells because of the reduced photocurrent. © 2016 Wiley Periodicals, Inc. J. Appl. Polym. Sci. **2016**, *133*, 44182.

KEYWORDS: dyes/pigments; functionalization of polymers; optical and photovoltaic applications

Received 5 April 2016; accepted 10 July 2016
DOI: 10.1002/app.44182

INTRODUCTION

Dye-sensitized solar cells (DSSCs) have attracted enormous interest as promising energy devices because of their cost-efficient fabrication, convenient process, and remarkable power-conversion efficiency.[1–4] As a critical component in DSSCs, sensitizers manage the responsibility of light capturing; thus, they play a crucial role in determining the overall performance of solar cells.[5] Recently, conjugated polymers have featured advantages of sufficiently large absorption coefficients, tunable band gaps spanning a broad portion of the visible and near-infrared spectrum, and excellent stability; this makes them promising candidates as active materials in DSSCs.[6–8] In this case, great efforts have been dedicated to the structural modification of polymer materials for DSSCs. Notably, only a few reports have discussed the influence of the molecular weights of the polymer dyes on the device performance.

Recently, Schanze and coworkers[9,10] produced several articles focusing on the use of novel donor–acceptor structured conjugated polymers as sensitizers in DSSCs. Their studies investigated the influence of polymer dye molecular weight on cell performance. The results were that the cell efficiency decreased with increasing molecular weight of the polymer dyes. This phenomenon was attributed to the long chain of the polymer sensitizers, which lowered their ability to diffuse into mesoporous TiO_2 films and to cover the surface effectively. However, in our previous work, we reported that poly(triphenylamine–phenothiazine) dyes with a large molecular weight of about 40 kg/mol exhibited relatively high power-conversion efficiencies, which exceeded 4%.[11] It follows that the potential for further exploration exists for polymer-sensitized solar cells to optimize their efficiency through the regulation of the molecular weight. Hence, it is of great importance to investigate the influence of the molecular weight of polymer dyes on the physical and electrochemical properties and photovoltaic performance of DSSCs.

Among the numerous reported organic dyes, triphenylamine-based dyes get a lot of attention in photovoltaic cells because of

Additional Supporting Information may be found in the online version of this article

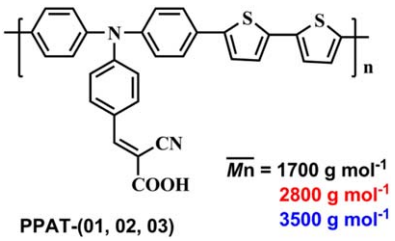

Figure 1. Structure of the oligomer dyes. [Color figure can be viewed in the online issue, which is available at wileyonlinelibrary.com.]

their excellent chemical and thermal stability and their good ability for form films.[12–15] Both theoretical and experimental studies have demonstrated that the triphenylamine unit contains electron-rich nitrogen with a high electron-donating ability, and its nonplanar propeller conformation can sufficiently inhibit the aggregation of dyes.[16] Recently, some groups[17–20] have reported that polymer-sensitized solar cells with triphenylamine-based polymers as sensitizers have shown acceptable power-conversion efficiencies of 2.1–4.7% under AM 1.5 irradiation. Our group has long been interested in the development of triphenylamine-based polymers sensitizers for solar cell applications.[11,19,20] In this study, we designed a series of oligomer dyes that featured the same conjugated backbone with alternating triphenylamine and 2,2′-bithiophene repeating units and researched the relationship between the overall cell efficiency and the dye's number-average molecular weight (M_n). The oligomer dyes were synthesized with a Stille coupling reaction, and the M_n values were controlled by selective polymerization times (Figure 1). Ultraviolet–visible (UV–vis) absorption spectra of the oligomer dyes were obtained to investigate their photophysical properties in solution and as adsorbed on TiO_2. DSSC devices based on these oligomer dyes were fabricated and examined for the effects of the M_n values on the photovoltaic performance properties.

EXPERIMENTAL

Materials

All reagents and solvents were analytical-grade quality and purchased commercially; they were used as received unless otherwise specified. Toluene and tetrahydrofuran (THF) were distilled over sodium/benzophenone. *N*,*N*-Dimethylformamide (DMF) was stirred with calcium hydride and distilled under reduced pressure. 2,2′-Bithiophene was purchased from Inno-Chem Science & Technology Co., Ltd. *N*-Bromosuccinimide (NBS), triphenylamine, cyanoacetic acid, piperidine, tri-*n*-butyltin chloride, and 1-bromo-4-methoxybenzene were purchased from Energy-Chemical and were used as received. Tetrakis(triphenylphosphine) palladium [$Pd(PPh_3)_4$], 1,3-dimethyl imidazole iodine, guanidine thiocyanate, and 4-*tert*-butylpyridine were purchased from Sigma-Aldrich. All reactions were carried out under nitrogen unless otherwise noted.

Synthesis

Synthesis of 4-(diphenylamino)benzaldehyde (1). Triphenylamine (12.3 g, 50.0 mmol) was dissolved in anhydrous DMF (24.3 g, 334 mmol) and stirred at 0 °C for 2 h. To the previous solution, phosphorus oxychloride (15.3 g, 100 mmol) was dropped. After that, the mixture was refluxed for 7 h at room temperature. The residue was poured into into an ice bath, neutralized with sodium bicarbonate, extracted with dichloromethane, and dried over magnesium sulfate. After the solvent was removed under reduced pressure, the crude product was purified over silica gel with petroleum ether/ethyl acetate (20:1 vol/vol) as the eluent to afford a yellow solid (8.68 g, yield = 67.0%).

^{1}H-NMR (400 MHz, $CDCl_3$, δ): 7.05 (d, J = 9.2, 2H), 7.30–7.40 (t, J = 7.2, 4H), 7.17–7.23 (m, 6H), 7.69 (d, J = 9.2, 2H), 9.89 (s, 1H). ^{13}C-NMR ($CDCl_3$, 400 MHz, δ): 190.44, 153.37, 146.17, 131.32, 129.76, 129.12, 126.33, 125.13, 119.37.

Synthesis of 4-[bis(4-bromophenyl)amino]benzaldehyde (M1). NBS (11.6 g, 65.3 mmol) was added to a solution of compound **1** (8.48 g, 31.1 mmol) in anhydrous THF (200 mL) and then stirred at 0 °C for 4 h. The solvent was removed, the residue was washed with water (150 mL) and saturated aqueous sodium chloride (100 mL), and the organic layer was dried over anhydrous magnesium sulfate. Then, the residue was purified by silica gel chromatography and eluted with petroleum ether/dichloromethane (4:1 vol/vol) to give a yellow solid (13.4 g, yield = 97.0%).

^{1}H-NMR (400 MHz, $CDCl_3$, δ): 7.45–7.50 (d, J = 8.8, 4H), 7.02–7.08 (m, 6H), 7.73 (d, J = 8.8, 2H), 9.86 (s, 1H). ^{13}C-NMR ($CDCl_3$, 400 MHz, δ): 190.39, 152.37, 145.04, 132.96, 131.42, 130.17, 127.42, 120.46, 118.11.

Synthesis of 5,5′-Bis(tributylstannyl)-2,2′-bithiophene (M2). A solution of 2,2′-bithiophene (9.98 g, 60.0 mmol) in anhydrous THF (80 mL) was cooled to −78 °C under nitrogen and stirred at this temperature for 30 min in a dried three-necked, round-bottom flask. *n*-Butyl lithium (*n*-BuLi; 60.0 mL of a 2.5 *M* solution in hexane, 150 mmol) was added dropwise with a syringe, and the mixture was stirred at −78 °C for 1 h. It was then warmed up to 0 °C for 30 min and cooled again to −78 °C. Tri-*n*-butyltin chloride (45.4 mL, 180 mmol) was added rapidly to the solution, and the resulting mixture was warmed to room temperature and stirred overnight. The reaction mixture was poured into water and extracted with dichloromethane. The combined organic layers were washed with a little brine and dried over magnesium sulfate, and the solvents were evaporated with a rotary evaporator. Column chromatography of the residue over neutral alumina with petrol ether as an eluant gave **M2** as a colorless liquid (31.3 g, yield = 70%).

Synthesis of precursor PPATCHO-01. In a 100-mL, three-necked round-bottom flask, a mixture of **M1** (1.98 g, 4.60 mmol), **M2** (2.17 g, 5.00 mmol), and $Pd(PPh_3)_4$ (0.53 g, 0.46 mmol) were dissolved in 40 mL of degassed toluene and deoxygenated with nitrogen for 30 min. The reaction mixture was stirred at 110 °C for 4 h, and then, an excess amount of 4-bromoanisole was added to end-cap the trimethylstannyl groups. After the reaction proceeded for 4 h, the mixture was cooled to 40 °C and added slowly into a vigorously stirred mixture of methanol. The polymers were collected by filtration and reprecipitation from methanol. The crude polymers were purified further through washing with methanol and hexane for 2 days in a Soxhlet apparatus to remove the oligomers and catalyst residues. Then, the product was extracted with chloroform

($CHCl_3$) for 24 h, and the solvent was removed by evaporation and finally vacuum-dried overnight. A yellow solid (0.88 g, yield = 44.0%) was obtained.

^{1}H-NMR ($CDCl_3$, 500 MHz, ppm, δ): 9.88 (s, 1H), 7.79–7.72 (d, 2H), 7.65–7.55 (m, 6H), 7.45–7.35 (m, 4H), 7.25–7.15 (m, 13H), 7.10–7.00 (d, 2H), 3.77 (s, 3H). Gel permeation chromatography (GPC): M_n = 1713 g/mol, weight-average molecular weight (M_w)/M_n = 1.3.

Synthesis of Precursor PPATCHO-02. The synthesis procedure for PPATCHO-02 was same as that for PPATCHO-01.The difference was that the time of the polymerization reaction was controlled at 24 h. After purification, a brown–orange solid was obtained (0.84 g, yield = 42.0%).

^{1}H-NMR ($CDCl_3$, 500 MHz, ppm, δ): 9.88 (s, 1H), 7.85–7.40 (m, 17H), 7.25–7.15 (m, 12H), 6.82–6.79 (d, 2H), 3.81 (s, 3H). GPC: M_n = 2852 g/mol, M_w/M_n = 1.7.

Synthesis of Precursor PPATCHO-03. The synthesis procedure for PPATCHO-03 was the same as that for PPATCHO-01.The difference was that the time of the polymerization reaction was controlled at 48 h. After purification, a brown–red solid was obtained (0.93 g, yield = 35.0%).

^{1}H-NMR ($CDCl_3$, 500 MHz, ppm, δ): 9.88 (s, 1H), 7.80–7.72 (m, 4H), 7.65–7.50 (m, 9H), 7.45–7.30 (m, 4H), 7.27–7.15 (m, 16H), 6.96–7.94 (d, 2H), 3.87 (s, 3H). GPC: M_n = 3846 g/mol, M_w/M_n = 1.3.

Synthesis of Dye Poly(triphenylamine-2,2′-bithiophene) Dye 01 (PPAT-01). To a solution of PPATCHO-01 (0.78 g, 1.79 mmol) and cyanoacetic acid (0.46 g, 5.37 mmol) in 30 mL of $CHCl_3$, piperidine (1.07 g, 12.5 mmol) was added dropwise under an N_2 atmosphere and refluxed at 85 °C for 24 h. After it was cooled to room temperature, the resulting mixture was poured into a 2 *M* hydrochloric acid solution (20 mL). $CHCl_3$ was used to extract the crude product, and the combined organic layer was washed with water three times and dried over magnesium sulfate. After the solvent was removed, the residue was dissolved in DMF and precipitated from diethyl ether to yield PPAT-01 as an orange–red solid (0.66 g, yield = 73.0%).

^{1}H-NMR [dimethyl sulfoxide (DMSO); 500 MHz, ppm, δ]: 12.1 (s, 1H), 8.2–7.0 (m, 27H), 3.81 (s, 3H).

Synthesis of Poly(triphenylamine-2,2′-bithiophene) Dye 02 (PPAT-02). The synthesis procedure for PPAT-02 was the same as that for PPAT-01. After purification, an orange–red solid was obtained (0.91 g, yield = 88.0%).

^{1}H-NMR (DMSO, 500 MHz, ppm, δ): 12.2 (s, 1H), 8.2–7.1 (m, 35H), 3.81 (s, 3H).

Synthesis of Poly(triphenylamine-2,2′-bithiophene) Dye 03 (PPAT-03). The synthesis procedure for PPAT-03 was the same as that for PPAT-01. After purification, a dark red solid was obtained (0.43 g, yield = 72.0%).

^{1}H-NMR (DMSO, 500 MHz, ppm, δ): 12.1 (s, 1H), 8.2–7.1 (m, 37H), 3.83 (s, 3H).

Instrumentation and Methods

The ^{1}H-NMR and ^{13}C-NMR spectra were collected on a Bruker AM 400 spectrometer with d-chloroform or d-DMSO as the solvent. GPC data were collected on a system composed of a Waters 1515 pump and a Waters 2414 refractive-index detector, with $CHCl_3$ as the eluent at a flow rate of 0.1 mL/min. The system was calibrated against linear narrow dispersed polystyrene standards in $CHCl_3$. Fourier transform infrared (FTIR) spectroscopy was collected with a Varian 1000 FTIR (scimitar series) spectrometer in the 400–4000-cm^{-1} region. Samples were prepared by the dispersal of the complexes in KBr and the compression of the mixtures to form disks.

The UV–vis spectra were measured with a Agilent model G1103A spectrophotometer. Emission spectra were recorded with a PerkinElmer LS55 luminescence spectrometer. The emitted light was detected with a Hamamatsu R928 red-sensitive photomultiplier. Cyclic voltammetry measurement was carried out on an RST 5000 electrochemical workstation equipped with a glassy carbon electrode as the working electrode, an Ag/Ag + electrode as the reference electrode, and a Pt electrode as the counter electrode. The measurements performed in the supporting electrolyte consisting of dyes were done in dry DMF mixed with 0.1 *M* tetrabutylammonium hexaflourophosphate ($TBAPF_6$). The reference electrode was internally calibrated with a ferrocene/ferrocenium (Fc/Fc+) redox couple as an internal reference. The TiO_2 films (12 μm in thickness) were sensitized for 12 h in the dyes solution and were used to measure the adsorbed dye amounts on the TiO_2 surface.

Computation

The ground-state geometries were optimized with the hybrid B3LYP function and a 6-31G** basis set; these have been widely used in the calculation of organic photoelectric materials.[21] The vertical excitation energies were calculated with time-dependent density functional theory at MPW1K/6-31G** levels.[22,23] The effect of the solvent (THF) on the geometries and absorption spectra were simulated by the C-PCM method.[24] All calculations were uploaded through telnet client software SSHSecureShellClient-3.2.9 and carried out with the Gaussian 03 program package.[25]

Fabrication of Solar Cells

A screen-printed double-layer film of interconnected TiO_2 particles was used as the mesoporous negative electrode. A 7 μm thick transparent layer of 20-nm titanium particles was first printed on a fluorine-doped SnO_2 conducting glass electrode, and the electrode was further coated by a 5 μm thick scattering layer of 400-nm titanium particles. The film thickness was measured by a benchtop Ambios XP-1 stylus profile meter. The active area of the TiO_2 film was about 0.28 cm^2. After sintering at 500 °C and cooling to 90 °C, the TiO_2 electrode was stained by immersion overnight in a 200 μg/mL solution of dye dissolved in a binary solvent of THF and acetonitrile (AN; volume ratio = 1:1). The dye-loaded TiO_2 electrode was then rinsed with AN, dried by air flow, and further assembled with a thermally platinized, fluorine-doped SnO_2 positive electrode by a 25 μm thick Surlyn (DuPont) hot-melt gasket. It was sealed up by heating. The internal space was perfused with liquid electrolyte with the aid of a vacuum backfilling system. The

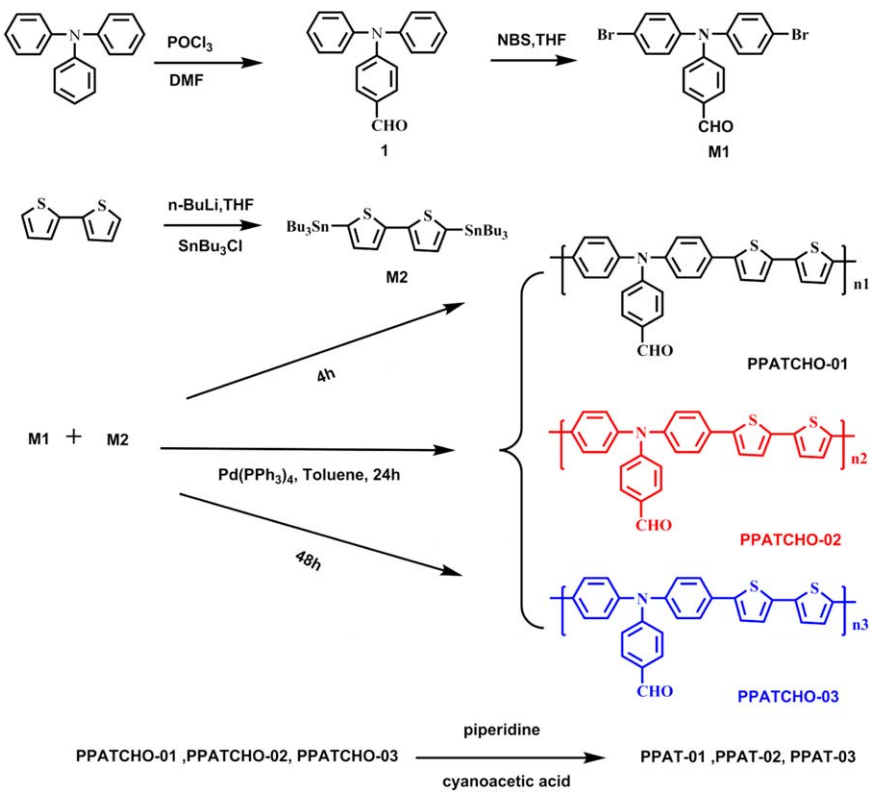

Scheme 1. Synthetic routes of the PPAT-01, PPAT-02, and PPAT-03 oligomer dyes. [Color figure can be viewed in the online issue, which is available at wileyonlinelibrary.com.]

electrolyte-injecting hole on the counter-electrode glass substrate, made with a sand-blasting drill, was sealed with a Bynel (DuPont) sheet and a thin glass covered by heating. Our iodine electrolyte was composed of 1.0 *M* 1,3-dimethyl imidazole iodine, 0.02 *M* iodine (I_2), 0.5 *M* 4-*tert*-butylpyridine, 0.1 *M* guanidine thiocyanate, and 0.05 *M* LiI in 3-methoxypropionitrile.

Photovoltaic Measurements

A Keithley 2400 source meter and a Zolix Omni-λ300 monochromator equipped with a 500-W xenon lamp were used for the measurements of the photocurrent action spectra. A Hamamatsu S1337 1010BQ silicon diode used for incident photon-to-current conversion efficiency (IPCE) measurements was calibrated at the National Institute of Metrology, China. A model LS1000 4S-AM 1.5G-1000-W solar simulator (Solar Light Co.) was used to give an irradiance of 100 mW/cm^2. The photocurrent–voltage (J–V) characteristics were obtained by the application of a bias potential to a testing cell and the measurement of photocurrent with a Keithley 2400 source meter under full computer control. An antireflection film ($\lambda < 380$ nm, ARKTOP, ASAHI Glass) was adhered to the DSSC photoanode during the IPCE and J–V measurements.

RESULTS AND DISCUSSION

Synthesis and Characterization

The detailed synthetic routes and characterization data of oligomer dyes are described in Scheme 1 and the Experimental section. In this study, PPAT-01, PPAT-02, and PPAT-03, which featured the same conjugated backbone with alternating triphenylamine and 2,2′-bithiophene repeating units, were synthesized. The monomer **M1** was synthesized with the first-step formylation of triphenylamine to obtain **1** and then bromination by NBS. The synthesis of **M2** was achieved according to a previous procedure.[26] The intermediates (**1**) and monomers (**M1** and **M2**) were characterized by ^{1}H-NMR. Three precursor dyes, PPATCHO-01, PPATCHO-02, and PPATCHO-03, were obtained through the palladium(0)-catalyzed Stille coupling reactions between the monomers **M1** and **M2** with different selected polymerization times (4, 24, and 48 h). Then, the monofunctional end-capping group 4-bromoanisole was added to the reaction mixture to end-cap the trimethylstannyl groups. The obtained precursor dyes were further purified by extraction on a Soxhlet apparatus with methanol and hexane for 48 h. Finally, $CHCl_3$ was used to dissolve the precursor dyes when the residue on the filter paper became colorless after 48 h, and the filtrates were dried under reduced pressure at room temperature. After purification and drying, all of the precursor dyes, PPATCHO-01, PPATCHO-02, and PPATCHO-03, were obtained in overall yields of 44, 42, and 35%, respectively. Then, the target dyes, PPAT-01, PPAT-02, and PPAT-03, were synthesized via the Knoevenagel condensation reaction between aldehyde and cyanoacetic acid in the presence of piperidine. All of the polymers fully dissolved in some common organic solvents, including THF, $CHCl_3$, toluene, and DMF, at room temperature after an ultrasonic treatment. The ^{1}H-NMR spectra of the oligomer dyes featured a strong resonance at 6.9–7.8 ppm with obvious coupling splitting. A weak resonance at 12.1 ppm confirmed the existence of —COOH groups. The spectra of the methoxyl

Table I. Molecular Weights of the Precursor Dyes PPATCHO-01, PPATCHO-02, and PPATCHO-03

Precursor dye	M_n (g/mol)[a]	M_w (g/mol)[a]	PDI	DP[a]	DP[b]	T_d (°C)[c]
PPATCHO-01	1713	2253	1.3	4	3	324
PPATCHO-02	2852	4834	1.7	5	5	280
PPATCHO-03	3486	4648	1.3	7	6	298

[a] Determined by GPC with polystyrene standards and with $CHCl_3$ as an eluent.
[b] Calculated by ^{1}H-NMR.
[c] T_d, 5% weight loss temperatures measured by thermogravimetric analysis under a nitrogen atmosphere.

group forms of the oligomers featured a resonance at a δ of 3.90 ppm; this confirmed the successful introduction of —OCH_3 end-capping groups into the oligomer frame.

Table I lists the M_n and M_w values and polydispersity indices (PDIs) of these oligomer dyes, as determined through GPC, against polystyrene standards in $CHCl_3$ as the eluent. The precursor dyes, PPATCHO-01, PPATCHO-02, and PPATCHO-03, were tested; we took into account the fact that the adsorption of the carboxyl group in GPC might have affected the test results. The results show that the M_n values of PPATCHO-01, PPATCHO-02, and PPATCHO-03 were 1713, 2852, and 3468 g/mol, and the PDI values were 1.3, 1.7, and 1.3, respectively. The degree of polymerization (DP) was also calculated by ^{1}H-NMR spectroscopy.[27,28] 4-Bromoanisole was selected as the monofunctional end-capping group, and the capping reaction is shown in Scheme 2.

The estimation of DP was based on the integral height ratio of aldehyde hydrogen in the precursor dyes and the methoxy hydrogen in equal number. The integral heights of —CHO and —OCH_3 are h_1 and h_2, respectively There was no interference between the two characteristic peaks. Thus, the DP could be calculated as follows:

$$\mathrm{DP}:1=(h_1/1):(h_2/3) \quad (1)$$

As shown in Table I, The results obtained by the GPC and NMR methods were in good agreement; this proved the precise M_n values of the oligomers. The three precursors, PPATCHO-01, PPATCHO-02, and PPATCHO-03, had relatively low molecular weights. This may have been due to the polymers' poor solubility in the solvent media because of their rigid main chains.

Figure 2 reveals the thermogravimetric analysis curves of PPAT-01, PPAT-02, and PPAT-03. Their 5% weight loss temperatures were 324, 280, and 298 °C, respectively; this indicated good thermal stability and potential use in device fabrication and application.

IR Spectra of the Dyes

The chemical structure messages of the oligomer dyes and **M1** monomer were revealed by FTIR spectroscopy measurements (Figure S2, Supporting Information). Typically, clear peaks at 512 cm^{-1} of **M1** were assigned to —C—Br stretching, and the absorption peaks at 2827 and 2740 cm^{-1} were assigned to the C—H stretching of —CHO. The disappearance of the absorption peak at 512 cm^{-1} and the appearance of the absorption peaks at 3062–3060 and 750 cm^{-1} suggested the existence of thiophene in PPAT-01. The FTIR bands located at 2923 and 2856 cm^{-1} corresponded to the —C—H stretching mode of —CH_3 and suggested the presence of a capping group. The peak at 1691–1690 cm^{-1} was attributed to the carboxyl stretching vibration peak, which had a lower absorption frequency due to conjugation with the double bond. The peak at 2216 cm^{-1} was attributed to the —C═N stretching vibration peak of cyano groups. The broad peaks around 3425 cm^{-1} might have been due to the hydroxyl stretching vibration peak from the carboxyl of the dye or the adsorbed moisture within the networks due to the high porosity. These results demonstrate the successful coupling chemistry.

Photophysical and Electrochemical Properties

The UV–vis absorption spectra of the three dyes, PPAT-01, PPAT-02, and PPAT-03, in THF solutions (200 μg mL^{-1}) are shown in Figure 3(a), and their corresponding properties are summarized in Table II. The absorption spectra of these sensitizers were characterized by two spectral features. The absorption peak around 280 nm was attributed to the π–π* transitions of their conjugated backbones, in which the absorption maximum (λ_{max}) of PPAT-01, PPAT-02, and PPAT-03 were 273, 279, and 282 nm, respectively. In addition, the absorption peak at about 450 nm was ascribed to the intramolecular charge transfer from the donor to the acceptor.[29–31] The absorption spectra for the three dyes were similar, with λ_{max} redshifting as the M_n values increased, and the extinction coefficients also gradually increased. The extension of the effective conjugation chain increased the extent of electron delocalization over the whole molecule and the ability of the dyes to donate electrons; thus, the λ_{max} peaks of these dyes were redshifted to 407, 413, and 428 nm for PPAT-01, PPAT-02, and PPAT-03, respectively.

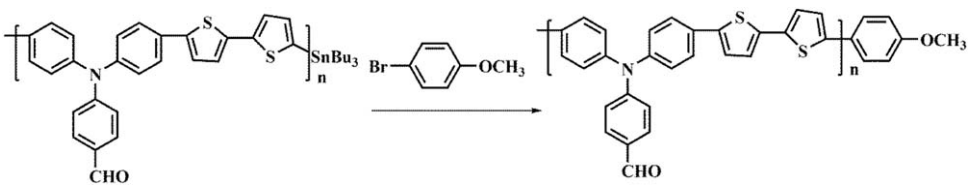

Scheme 2. End-capping reaction of the precursor dyes.

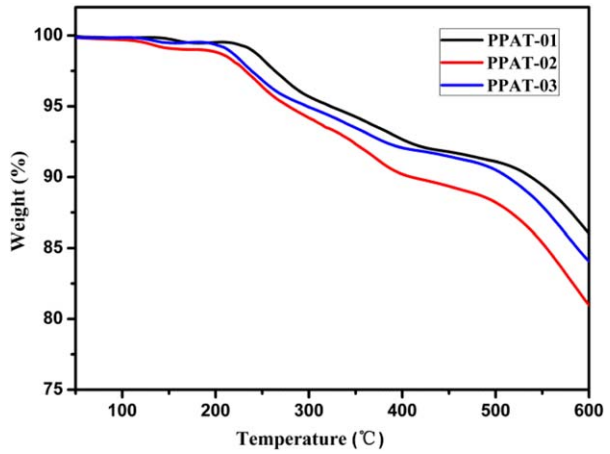

Figure 2. Thermogravimetric analysis curves of the PPAT-01, PPAT-02, and PPAT-03 dyes at a heating rate of 10 °C/min under an N_2 atmosphere. [Color figure can be viewed in the online issue, which is available at wileyonlinelibrary.com.]

When the dyes were adsorbed on the TiO_2 films, the absorption spectra maxima of these dyes were 404, 409, and 403 nm, respectively. Compared with the solution absorption, the absorption bands of the dyes on the TiO_2 films were blueshifted [Figure 3(b)]; this indicated that some interactions existed between the dyes and the TiO_2 surface. For PPAT-01 and PPAT-02, the absorption spectra blueshifted slightly (ca. 3 and 4 nm); this was mainly ascribed to the deprotonation of carboxylic acid. However, for PPAT-03, the large blueshift (ca. 25 nm) on TiO_2 compared with that in solution indicated that the dyes had a greater tendency to form aggregates on TiO_2, especially H aggregates.[32–34]

The amount of the oligomer dyes absorbed on the TiO_2 films was estimated by the measurement of changes in absorbance of the dye solutions before and after adsorption. The TiO_2 surface concentrations of PPAT-01, PPAT-02, and PPAT-03 sensitized in the THF/AN (1:1) mixed solvent on the TiO_2 surface were determined to be 3.1×10^{-7}, 1.7×10^{-7}, and 0.8×10^{-7} mol cm^{-2} μm^{-1}, respectively. The adsorbed amount decreased when the molecular weight of the oligomer dyes increased. The amount of PPAT-03 adsorbed on TiO_2 was very low; this led to a narrow action spectrum and a decreased photocurrent.

As illustrated in Figure 4, the three dyes, PPAT-01, PPAT-02, and PPAT-03, exhibited fluorescence in the visible region, and the corresponding emission maxima are summarized in Table II. PPAT-03 demonstrated a strong fluorescence with a λ_{max} of 490 nm and a Stokes shift of about 62 nm; this indicated a strong intrachain charge-transfer character in the singlet excited state. The fluorescence spectrum of the polymer dyes PPAT-01 and PPAT-02 blueshifted relative to that of PPAT-03. Specifically, PPAT-01 exhibited weak fluorescence, with a λ_{max} of 469 nm, and PPAT-02 also exhibited weak fluorescence, with a λ_{max} of 474 nm. The Stoke redshifts suggested an existent energy loss upon photoexcitation;[9] this was most possibly due to the twisted diphenylamine side chain or triphenylamine–cyanoacetic acid interaction and/or intramolecular charge transfer.

Electrochemical Properties

To evaluate the possibility of electron injection and dye regeneration on the conduction band of TiO_2, cyclic voltammetry was performed in DMF solution (Figure 5) with a Fc/Fc + redox couple as an external standard to determine the redox potential. The electronic energy levels of PPAT-01, PPAT-02, and PPAT-03 were calculated from the onset potentials of the onset oxidation potentials (E_{ox}).[35] The E_{ox} values were 0.56 for PPAT-01, 0.78 V for PPAT-02, and 0.63 V for PPAT-03. The highest occupied molecular orbital (HOMO) energy levels E_{HOMO} of these dyes were estimated according to the following equation[23]:

$$E_{HOMO} = -[E_{ox} - E(Fc/Fc^{+}) + 4.8]eV \quad (2)$$

The HOMO and lowest unoccupied molecular orbital (LUMO) levels of these dyes are summarized in Table II. The HOMO levels of PPAT-01, PPAT-02, and PPAT-03 (−4.98, −5.13, and −4.89 eV, respectively) were more negative than that of I^-/I_3^- (−4.6 eV). This ensured the thermodynamic regeneration of the oxidized dyes. As estimated from the band gap derived from the intersection points of the normalized absorption and emission spectra, the resulting optical band gap E_{0-0} values were 2.76, 2.73, and 2.61 eV for PPAT-01, PPAT-02, and PPAT-03, respectively (Figure 6). Consequently, all of the LUMO levels of these

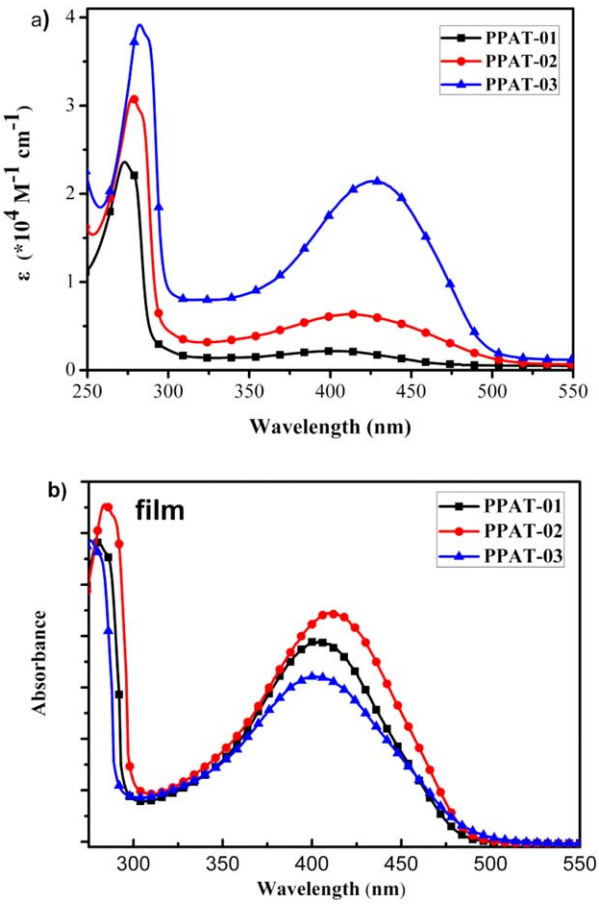

Figure 3. (a) Absorption spectra of PPAT-01, PPAT-02, and PPAT-03 in THF and (b) absorption spectra of PPAT-01, PPAT-02, and PPAT-03 anchored onto TiO_2 films. ε, the extinction coefficient. [Color figure can be viewed in the online issue, which is available at wileyonlinelibrary.com.]

Table II. Photophysical and Electrochemical Data for PPAT-01, PPAT-02, and PPAT-03

Oligomer dye	λ_{max} (nm)[a]	ε_{max}[g] (10^4 M^{-1} cm^{-1})[a]	λ_{max} (nm)[b]	λ^{PL}_{max}(mn)[c]	E_{0-0} (eV)[d]	HOMO (eV)[e]	LUMO (eV)[f]
PPAT-01	273,407	2.35, 0.20	404	469	2.76	−4.98	−2.22
PPAT-02	279,413	3.08, 0.62	409	474	2.73	−5.13	−2.40
PPAT-03	282,428	3.91, 2.13	403	490	2.61	−4.89	−2.28

[a] Absorption spectra in THF.
[b] Adsorbed on the TiO_2 films.
[c] Fluorescence spectra in THF.
[d] Optical band gap determined from the absorption onset.
[e] Determined by cyclic voltammetry: HOMO = $-[E_{ox} - E(Fc/Fc^+) + 4.8]$ eV and $E(Fc^+/Fc) = 0.4$ V.
[f] LUMO = HOMO − E_{0-0}.
[g] ε_{max} the maximum extinction coefficient.

dyes (−2.22, −2.40, and −2.28 eV, respectively) were more positive than that of the conduction band of TiO_2. This provided a sufficient driving force for electron injection from the oxidized organic dyes to TiO_2. From this value, we found that PPAT-02 showed a more negative HOMO level than PPAT-01 and PPAT-03 (Figure 7); this indicated a strong ability to regenerate and prevent the occurrence of side reactions.

Theoretical Calculations

To explore the possible distribution of electronic cloud and energy levels, density functional theory calculations were performed on the B3LYP/6-31G** level with Gaussian 03 to calculate the optimized molecular structures and frontier molecular orbitals of the oligomer dyes PPAT-01, PPAT-02, and PPAT-03 (Figure 8). The electronic density was mainly distributed into the donor units of triarylamine and bithiophene at the HOMO levels. The electrons in the LUMO levels of these dyes were mainly distributed over the anchoring group and phenyl moiety. Thus, the absorption leading to the electronic excitation from the HOMO to the LUMO energy level constituted the charge transfer from the donor units to the cyanoacrylic acid acceptor. This ensured charge separation in the molecule after light irradiation and subsequent efficient electron injection into the TiO_2 layer.[36] Figure 9 summarizes the calculated HOMO and LUMO levels of the dyes and the energy levels of TiO_2 and I^-/I_3^-. The HOMO and LUMO energy levels calculated for the dyes were not expected to display a disorderly change with the molecular weight increase; this was consistent with the experimentally observed values because the HOMO and LUMO levels were randomly and irregularly located on part of the donor and

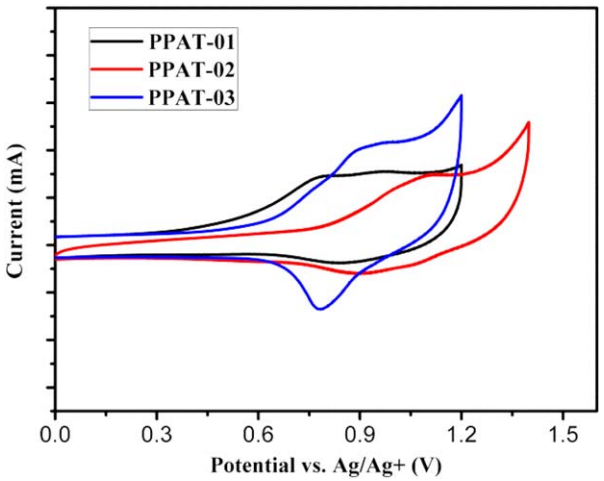

Figure 5. Cycle voltammograms of the PPAT-01, PPAT-02, and PPAT-03 dyes in THF with 0.1 *M* $TBAPF_6$. [Color figure can be viewed in the online issue, which is available at wileyonlinelibrary.com.]

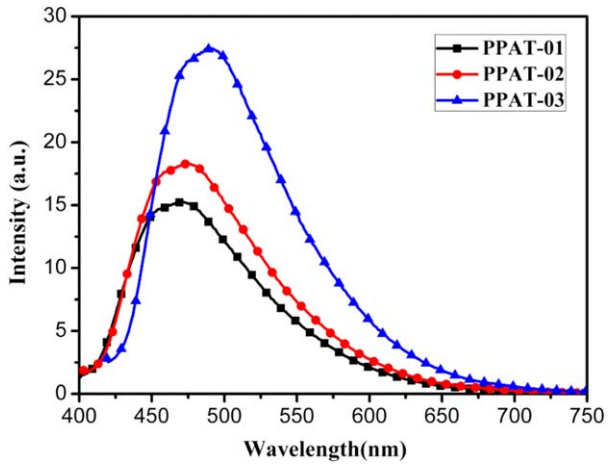

Figure 4. Emission spectra of the PPAT-01, PPAT-02, and PPAT-03 dyes in THF. [Color figure can be viewed in the online issue, which is available at wileyonlinelibrary.com.]

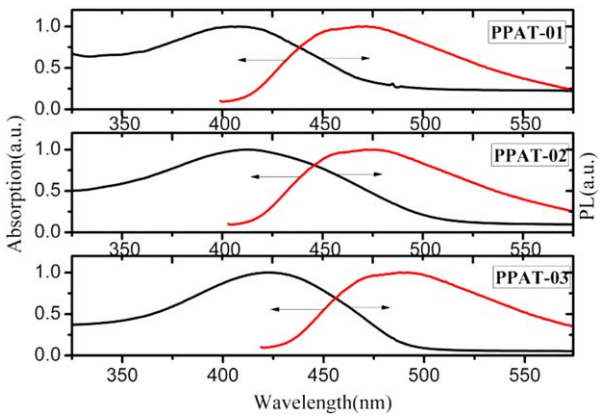

Figure 6. Normalized electronic absorption and emission spectra of the PPAT-01, PPAT-02, and PPAT-03 dyes in THF. [Color figure can be viewed in the online issue, which is available at wileyonlinelibrary.com.]

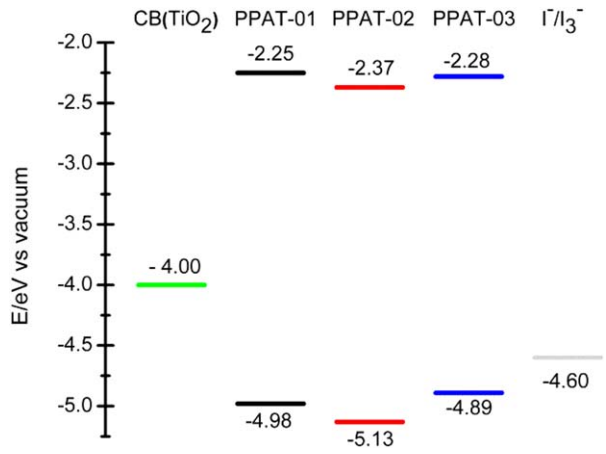

Figure 7. Comparison of the energy levels of the PPAT-01, PPAT-02, and PPAT-03 dyes dissolved in DMF in the ground and excited states. CB: conductive band. [Color figure can be viewed in the online issue, which is available at wileyonlinelibrary.com.]

acceptor units. Meanwhile, unlike small-molecule organic dyes with single-component oligomer dyes, PPAT series are mixtures composed of complicated analogues. Thus, the influence factors of energy levels for oligomer dyes are not simply small molecules.

Photovoltaic Performance of DSSCs

Figure 10 shows the IPCE plots as a function of the incident wavelength for DSSCs based on the oligomer dyes. The IPCE onsets for PPAT-01, PPAT-02, and PPAT-03 were 600, 650, and 575 nm, respectively, increasing in the order PPAT-03 < PPAT-01 < PPAT-02. The IPCE spectra were in good accordance with their absorption spectra on the TiO_2 film [Figure 3(b)]. The IPCE of PPAT-02 was higher than 50% in the range 400–500 nm, with a maximum value of 61% at 440 nm. It seemed that large molecular weight in PPAT-02 broadened the spectrum of absorption to get a better IPCE. Compared to PPAT-02, the IPCE of PPAT-01 was lower; this was due to weak light harvesting. In the case of PPAT-03, the corresponding IPCE value became quite lower. In solution, the continuous increase in the molecular weights of dyes broadened the conjugation length.

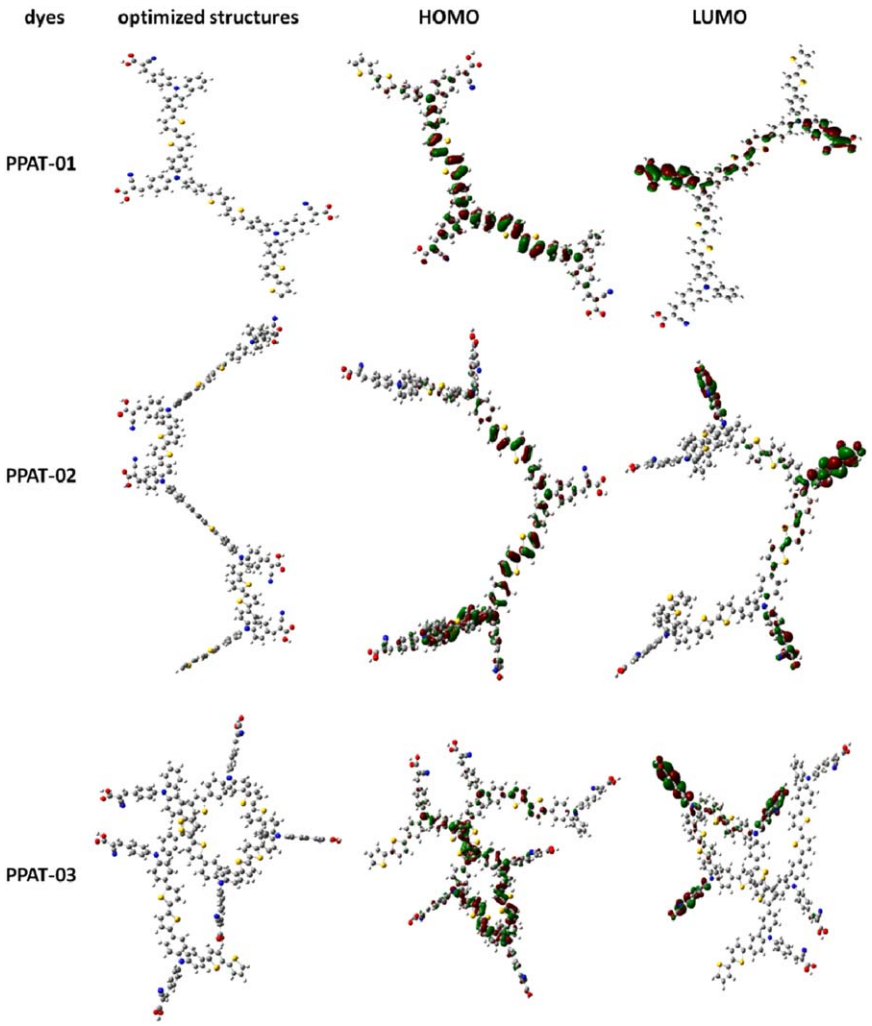

Figure 8. Molecular orbital distributions of PPAT-01, PPAT-02, and PPAT-03. The yellow, blue, and red symbols represent sulfur, nitrogen, and oxygen atoms, respectively. [Color figure can be viewed in the online issue, which is available at wileyonlinelibrary.com.]

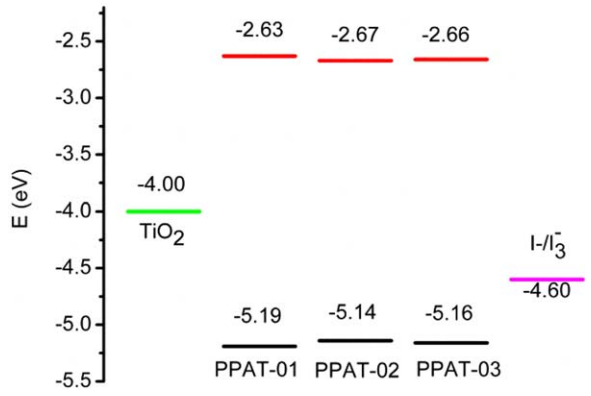

Figure 9. Energies of the frontier molecular orbitals of the PPAT-01, PPAT-02, and PPAT-03 dyes computed at the density functional theory/B3LYP/6-31G** level. [Color figure can be viewed in the online issue, which is available at wileyonlinelibrary.com.]

However, PPAT-03 formed H aggregates when adsorbed on the TiO_2 surface; this led to inefficient electron injection and decreased the photocurrent. Meanwhile, the decrease in the PPAT-03 adsorbed amount led to a narrowing action spectrum and a decrease in the IPCE value.

The typical J–V curves of the devices based on PPAT-01, PPAT-02, and PPAT-03 were evaluated under 100 mW/cm^2 simulated AM 1.5G solar light, as shown in Figure 11. The performances of the cells in terms of the open-circuit voltage (V_{oc}), short-circuit photocurrent density (J_{sc}), fill factor (FF), and power-conversion efficiency values are summarized in Table III. Among these dyes, the cell based on PPAT-02 exhibited the highest overall conversion efficiency (η) of 4.72% ($J_{sc} = 10.70$ mA/cm^2, $V_{oc} = 0.71$ V, FF = 0.69); this was mainly attributed to enhanced light harvesting. This arose from the increase in the molecular weight. Other cells sensitized with the dyes PPAT-01 and PPAT-03 showed relatively low performances with η values of 2.81 and 1.88%, respectively. We found that J_{sc} increased from 6.23 to 10.7 mA/cm^2 for PPAT-01 and PPAT-02 when the molecular weight increased from 1713 to 2852 g/mol. This was

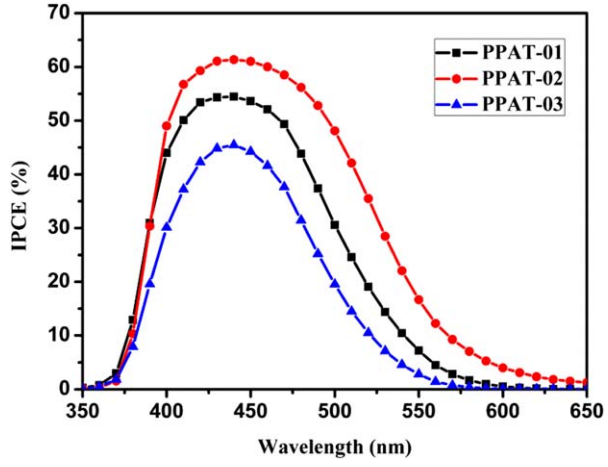

Figure 10. IPCE action spectra of the DSSCs sensitized by the PPAT-01, PPAT-02, and PPAT-03 dyes. [Color figure can be viewed in the online issue, which is available at wileyonlinelibrary.com.]

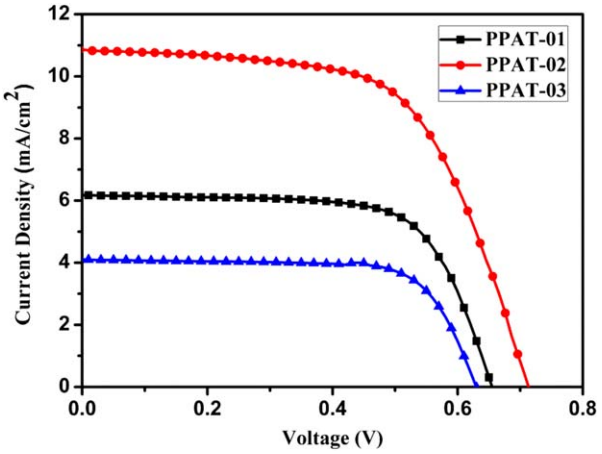

Figure 11. J–V characteristics measured under irradiation of 100 mW/cm^2 for more than 15 cells with simulated AM 1.5 sunlight. [Color figure can be viewed in the online issue, which is available at wileyonlinelibrary.com.]

Table III. Photovoltaic Parameters of Cells Measured at an Irradiation of 100 mW/cm^2 with Simulated AM 1.5 Sunlight

Oligomer dye	J_{sc} (mA/cm^2)	V_{oc} (V)	FF (%)	η (%)
PPAT-01	6.23 ± 0.28	0.65 ± 0.02	69 ± 3	2.81 ± 0.10
PPAT-02	10.7 ± 0.31	0.71 ± 0.02	61 ± 5	4.72 ± 0.10
PPAT-03	4.09 ± 0.26	0.63 ± 0.02	72 ± 2	1.88 ± 0.15

assigned to enhanced light harvesting with extended conjugated chains. However, a further increase in chain length results in decreasing η for PPAT-03. One reason for this phenomenon was that a small amount of dye adsorption for PPAT-03 led to interfacial charge recombination; this resulted in a decrease in V_{oc}. On the other hand, the formation of H aggregates in PPAT-03 led to a decrease in the photocurrent and poor performance of the DSSC-based dye.

CONCLUSIONS

In summary, a series of simple oligomer dyes with different molecular weights were synthesized and used as sensitizers in DSSCs. The results obtained by GPC and NMR methods demonstrated that the molecular weight was successfully controlled by the selection of the polymerization time for 4, 24, and 48 h. In this study, an unconventional correlation between the oligomer dye molecular weight and cell performance was demonstrated. With a further increase in the molecular weight, the cell efficiency of these dyes did not bring about a monotonic increase or decrease. The cell based on PPAT-02 displayed the highest η value than those based on PPAT-01 and PPAT-03. The photophysical comparison results of UV–vis absorption in solution and on the surface of TiO_2 revealed that PPAT-01 and PPAT-02 were adsorbed on TiO_2 with a monolayer state, whereas PPAT-03 formed a certain degree of H aggregates on the TiO_2. The polymer aggregates were very important factors in the photovoltage and photocurrent because less aggregated samples increased the effective surface coverage and suppressed

interfacial charge recombination in the liquid electrolyte DSSCs. Moreover, the adsorbed amount of oligomer dyes also affected the photoelectric performance, such as the light-harvesting capacity and electron transportation. These findings offer the possibility for using synthetic methods to control the chain length of the polymer dyes for applications in the DSSCs. However, there are still some issues that need to be solved, such as the directional assembly and adsorption form of polymer dyes on TiO_2. This may be another significant factor affecting the cell efficiency.

ACKNOWLEDGMENTS

This work was financially supported by the National Science Foundation of China (contract grant numbers 21204103 and 21376272), the China Postdoctoral Science Foundation (contract grant number 2012M521535), the China Postdoctoral Science Foundation Specialized Funded Project (contract grant number 2014T70787), and the State Key Laboratory of Fine Chemicals (contract grant number KF1206).

REFERENCES

1. O'regan, B.; Grätzel, M. *Nature* **1991**, *353*, 737.
2. Grätzel, M. *Acc. Chem. Res.* **2009**, *42*, 1788.
3. Calogero, G.; Di Marco, G.; Caramori, S.; Cazzanti, S.; Argazzi, R.; Bignozzi, C. A. *Energy Environ. Sci.* **2009**, *2*, 1162.
4. Yang, J. B.; Ganesan, P.; Teuscher, J.; Moehl, T.; Kim, Y. J.; Yi, C. Y.; Comte, P.; Pei, K.; Holcombe, T. W.; Nazeeruddin, M. K.; Hua, J. L.; Zakeeruddin, S. M.; Tian, H.; Grätzel, M. *J. Am. Chem. Soc.* **2014**, *136*, 5722.
5. Hagfeldt, A.; Boschloo, G.; Sun, L. C.; Kloo, L.; Pettersson, H. *Chem. Rev.* **2010**, *110*, 6595.
6. Yanagida, S.; Senadeera, G. K. R.; Nakamura, K.; Kitamura, T.; Wada, Y. *J. Photochem. Photobiol. A* **2004**, *166*, 75.
7. Chhatre, S.; Agarkar, S.; Dhas, V.; Nagane, S.; Thakare, V.; Ogale, S.; Wadgaonkar, P. *J. Mater. Chem.* **2012**, *22*, 23267.
8. Mwaura, J. K.; Zhao, X.; Jiang, H.; Schanze, K. S.; Reynolds, J. R. *Chem. Mater.* **2006**, *18*, 6109.
9. Fang, Z.; Eshbaugh, A. A.; Schanze, K. S. *J. Am. Chem. Soc.* **2011**, *133*, 3063.
10. Pan, Z.; Leem, G.; Cekli, S.; Schanze, K. S. *ACS Appl. Mater. Interfaces* **2015**, *7*, 16601.
11. Wang, G.; Wu, Y. Y.; Ding, W. H.; Yu, G. P.; Hu, Z. B.; Wang, H. Z.; Liu, S. Q.; Zou, Y. P.; Pan, C. Y. *J. Mater. Chem. A* **2015**, *3*, 14217.
12. Tian, H.; Yang, X.; Pan, J.; Chen, R.; Liu, M.; Zhang, R.; Hagfeldt, A.; Sun, L. *Adv. Funct. Mater.* **2008**, *18*, 3461.
13. Luo, J.; Wu, W. J.; Mu, J. S.; Wang, C.; Bai, X. D.; Wang, W. *J. Appl. Polym. Sci.* **2012**, *125*, 200.
14. Wang, Q.; Zakeeruddin, S.; Cremer, J.; Bauerle, P.; Humphry-Baker, R.; Grätzel, M. *J. Am. Chem. Soc.* **2005**, *127*, 5706.
15. Zhang, F.; Luo, Y.; Song, J.; Guo, X.; Liu, W.; Ma, C.; Meng, Q. *Dyes Pigments* **2009**, *81*, 224.
16. Bonhote, P.; Moser, J.; Humphry-Baker, R.; Vlachopoulos, N.; Zakeeruddin, S.; Walder, L.; Grätzel, M. *J. Am. Chem. Soc.* **1999**, *121*, 1324.
17. Zhang, W.; Fang, Z.; Su, M.; Saeys, M.; Liu, B. *Macromol. Rapid Commun.* **2009**, *30*, 1533.
18. Fang, Z.; Wu, D. L.; Keinan, S.; Liu, B. *Polym. Chem.* **2014**, *52*, 2958.
19. Tan, H. J.; Pan, C. Y.; Wang, G.; Wu, Y. Y.; Zhang, Y. P.; Chen, X.; Zou, Y. P.; Yu, G. P.; Zhang, M. *RSC Adv.* **2013**, *37*, 16612.
20. Wang, G.; Ding, W. H.; Wang, H. Z.; Zhou, X. Y.; Yu, G. P.; Pan, C. Y. *Synth. Met.* **2015**, *209*, 119.
21. Zhang, W.; Chen, X.; Liang, W.; Zhao, Y. *Commun. Comput. Chem.* **2013**, *1*, 132.
22. Lynch, B.; Fast, P.; Harris, M.; Truhlar, D. *J. Phys. Chem. A* **2000**, *104*, 4811.
23. Pastore, M.; Mosconi, E.; De Angelis, F.; Graätzel, M. *J. Phys. Chem. C* **2010**, *114*, 7205.
24. Cossi, M.; Rega, N.; Scalmani, G.; Barone, V. *J. Comput. Chem.* **2003**, *24*, 669.
25. Cai, N.; Wang, Y.; Xu, M.; Fan, Y.; Li, R.; Zhang, M.; Wang, P. *Adv. Funct. Mater.* **2013**, *23*, 1846.
26. Sahu, D.; Padhy, H.; Patra, D.; Huang, J. H.; Chu, C. W.; Lin, H. C. *Polym. Chem.* **2010**, *48*, 5812.
27. Gao, Y.; Jian, X. G. *Polym. Mater. Sci. Eng.* **1999**, *15*, 167.
28. Ding, J.; F'Price, C. H. *Eur. Polym. J.* **1991**, *27*, 895.
29. Huang, F.; Chen, K.; Yip, H.; Hau, S. K.; Acton, O.; Zhang, Y.; Luo, J.; Jen, A. K. *J. Am. Chem. Soc.* **2009**, *131*, 13886.
30. Zhang, Z.; Zhang, K.; Liu, G.; Zhu, C.; Neoh, K.; Kang, E. *Macromolecules* **2009**, *42*, 3104.
31. Leriche, P.; Frère, P.; Cravino, A.; Alévêque, O.; Roncali, J. *J. Org. Chem.* **2007**, *72*, 8332.
32. Tian, H. N.; Yang, X. C.; Chen, R. K.; Zhang, R.; Hagfeldt, A.; Sun, L. *J. Phys. Chem. C* **2008**, *112*, 11023.
33. Lin, L. Y.; Tsai, C. H.; Wong, K. T.; Huang, T. W.; Hsieh, L.; Liu, S. H.; Lin, H. W.; Wu, C. C.; Chou, S. H.; Chen, S. H.; Tsai, A. I. *J. Org. Chem.* **2010**, *75*, 4778.
34. Thomas, K. R. J.; Hsu, Y. C.; Lin, J. T.; Lee, K. M.; Ho, K. C.; Lai, C. H.; Cheng, Y. M.; Chou, P. T. *Chem. Mater.* **2008**, *20*, 1830.
35. Li, Y.; Cao, Y.; Gao, J.; Wang, D.; Yu, G.; Heeger, A. *J. Synth. Met.* **1999**, *99*, 243.
36. Kumar, D.; Justin Thomas, K. R.; Lee, C. P.; Ho, K. C. *J. Org. Chem.* **2014**, *79*, 3159.